# Nanoscale ridge aperture as near-field transducer for heat-assisted magnetic recording

Nan Zhou, Edward C. Kinzel, and Xianfan Xu*

School of Mechanical Engineering and Birck Nanotechnology Center, Purdue University, West Lafayette, Indiana 47906, USA

*Corresponding author: xxu@purdue.edu

Received 21 July 2011; accepted 18 August 2011;
posted 29 August 2011 (Doc. ID 151340); published 7 October 2011

Near-field transducer based on nanoscale optical antenna has been shown to generate high transmission and strongly localized optical spots well below the diffraction limit. In this paper, nanoscale ridge aperture antenna is considered as near-field transducer for heat-assisted magnetic recording. The spot size and transmission efficiency produced by ridge aperture are numerically studied. We show that the ridge apertures in a bowtie or half-bowtie shape are capable of generating small optical spots as well as elongated optical spots with desired aspect ratios for magnetic recording. The transmission efficiency can be improved by adding grooves around the apertures. © 2011 Optical Society of America

*OCIS codes:* 210.4770, 050.1220, 240.6680.

## 1. Introduction

Heat-assisted magnetic recording (HAMR) is a promising technique to increase the storage density of the next generation hard disk drives [1]. As the storage density continues to increase, one of the problems is that the magnetic medium must be made of materials with a very high coercivity, requiring a magnetic field beyond what can be supplied by the hard disk head. HAMR solves this problem by raising the temperature of the magnetic medium above the Curie temperature using laser heating and temporarily and locally lowering the coercivity of the medium. One of the most difficult challenges in developing the HAMR system is to deliver sufficient laser power into the recording medium within a spot well below the diffraction limit. For example, to achieve a storage density of the order of $1\,\mathrm{Tb/in.}^2$ (1 terabits per square inch), an optical spot of about 25 nm × 25 nm is required. A number of methods are being investigated, including the use of solid immersion-based optical systems [2–5] and near-field transducers (NFT) [6–9]. The former approach can focus light to a spot of about $\lambda/4$ and deliver efficient energy to the transducer. The NFT further reduces the optical spot size with efficient energy transmission to the lossy recording medium. In this study, we focus on the discussion of the optical spot size and efficiency produced by NFT.

Nanoscale optical antennas are the most frequently used NFTs for their abilities to overcome the diffraction limit. It is shown that these nanostructures can reduce the optical spots to a range of 30 nm–50 nm [7]. A special type of NFT design in the shape of a "lollipop" is shown to have a strong interaction with the recording medium [8]. High optical efficiency is desirable, as most of the energy is lost during the delivery, which could lead to heating of the recording head, head deformation, and component failure [10]. Designing NFT using aperture-type optical antennas is quite advantageous in this regard since they can better transfer heat away from the transducer [7]. In our study, we focus on the spot size and transmission efficiency produced by three types of ridge aperture antennas: the bowtie aperture, half-bowtie aperture, and *C* aperture antennas. We also show that the transmission efficiency can be improved by adding grooves around the apertures.

0003-6935/11/310G42-05$15.00/0
© 2011 Optical Society of America

## 2. Simulation Model

Numerical analyses are performed using a frequency-domain finite-element method (FEM) solver [11]. Figure 1 illustrates the simulation model on the $yz$ plane and the three types of apertures in the $xy$ plane. Silver film with a thickness of $t$ is used, as shown in Fig. 1(a). The composition, thicknesses, and optical properties [12] of the recording media stack are summarized in Table 1. The 800 nm wavelength is used, which is close to that of a diode laser used for HAMR. Each aperture is defined by the outline dimensions $a$ and $b$. $s$ and $d$ define the length and width of the air gap. The flare angles are fixed at 45° and the corners are rounded to represent the actual manufactured geometry for bowtie and half-bowtie apertures [shown for bowtie aperture as an example in Fig. 1(b)]. A normally incident Gaussian beam from the substrate side is applied to excite the aperture. It has a beam waist $w$ of 1 $\mu$m and is polarized along the $y$ direction. The transmission efficiency is computed as the ratio of the power on the exit side of the film to the power contained in the incident Gaussian beam $P_0$, expressed as

$$P_0 = \pi/2\frac{E_0^2}{2\eta}w^2, \tag{1}$$

where $E_0$ and $\eta$ are the peak electric field amplitude and characteristic impedance in the substrate, respectively. To compute the absorption density $q$ (in a unit of W/m$^3$) in the recording medium, the FePt layer, we use a peak electric field amplitude in the quartz substrate as $E_0 = 1/1.453$ V/m, which corresponds to a peak intensity of $I_0 = E_0^2/2\eta = 0.9135$ mW/m$^2$ and an incident power of $P_0 = 1.435 \times 10^{-15}$ W. These numbers are arbitrarily chosen for the purpose of comparing absorption density using different designs. The absorption density $q$ is defined as

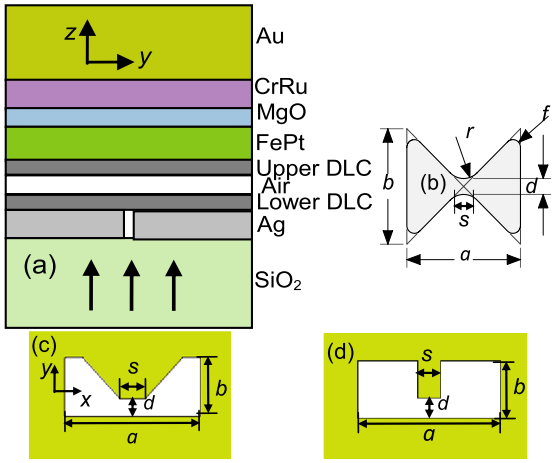


Fig. 1. (Color online) Geometry of the aperture NFTs. (a) Cross-sectional view of the media stack, (b) bowtie aperture (the outer corners are filleted with a radius $f = 5$ nm and the inner corners with a radius $r = 2$ nm), (c) half-bowtie aperture, and (d) $C$ aperture.

Table 1. Thicknesses and Optical Properties of the Media Stack

| material | thickness [nm] | $n$ | $k$ |
|---|---|---|---|
| $SiO_2$ | $\infty$ | 1.453 | 0 |
| Ag | $t$ | 0.036 | 5.566 |
| Upper DLC | 1 | 1.53 | 0 |
| Air | 2 | 1 | 0 |
| Lower DLC | 1 | 1.53 | 0 |
| FePt | 8 | 3.3 | 4.3 |
| MgO | 5 | 1.76 | 0 |
| CrRu | 15 | 3.15 | 5.68 |
| Au | 50 | 0.154 | 4.908 |

$$q = 1/2\mathrm{Re}(\vec{E}\cdot\vec{J}^{*} + jw\vec{B}\cdot\vec{H}^{*}), \tag{2}$$

where $\vec{J}^{*}$ is the conjugate of the volumetric current density and $H$ is the conjugate of the magnetic field.

## 3. Results and Discussion

### A. Generating Subdiffraction Limited Heat Spots Using Nanoscale Bowtie Apertures

Bowtie apertures have been demonstrated to concentrate and enhance optical fields [13,14], with applications including near-field scanning microscopy (NSOM) measurements [15] and nanolithography [16–18]. In this section, we apply bowtie apertures to the HAMR system to obtain subdiffraction limited heat spots.

We first fix the outline dimension of the bowtie aperture as 200 nm × 200 nm and the thickness $t$ of the Ag film as 100 nm and evaluate the effect of the gap size $d$ of the aperture. Silver is chosen since it has the most suitable properties for obtaining high intensity near-field spot. The size of the optical spot generated by the bowtie aperture is almost entirely dictated by the gap dimension. Figure 2(a) shows the full-width at half-maximum (FWHM) of the heat spot as a function of the gap size, which increases almost linearly with the gap. For a gap size of 5 nm, the smallest used in the calculation, the FWHM of the spot is 19.4 nm($x$) × 18.6 nm($y$). Figures. 2(b) and 2(c) show absorption densities at the entrance surface of the FePt layer for different aperture gaps. It is seen that the absorption density decreases with the increase of the gap size.

We then optimize the aperture size and thickness to maximize the absorption density in the recording medium. This is equivalent to impedance matching when the aperture is considered a short section of waveguide. Figure 3(a) shows how the absorption density in the surface of the FePt layer directly above the aperture center varies with the outline dimension and thickness of the bowtie aperture. The best results are achieved at $a = b = 500$ nm and $t = 100$ nm. Figures 3(b) and 3(c) show the absorption at different depths into the FePt layer under these dimensions. A large gradient of absorption density is obtained in the medium.

Results in Figs. 3(a)–3(c) are obtained for the gap size $d = 5$ nm; results obtained using other gap sizes

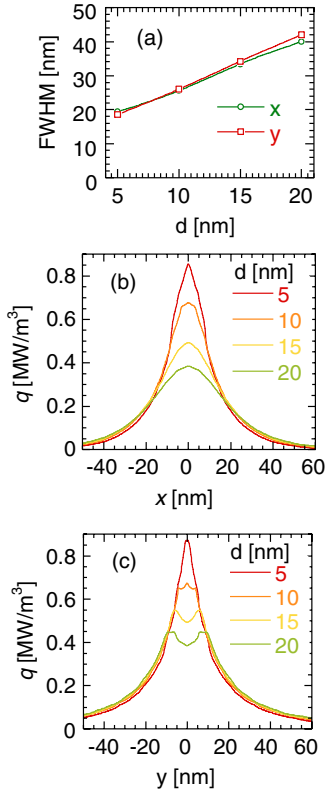


Fig. 2. (Color online) (a) FWHM in $x$ and $y$ directions as a function of aperture gap $d$. The spot sizes are calculated at the entrance surface of the FePt layer, which is 4 nm from the exit side of the aperture. Heat generation in (b) the $x$ direction and (c) the $y$ direction.

have the same trends. For $d = 5$ nm, the largest transmission efficiency is 2.1% at $a = b = 500$ nm and $t = 100$ nm. The transmitted power is evaluated on the exit side of the aperture with a circular region whose radius is 40 nm. The use of a circular region with a 40 nm radius is to exclude the light that is not localized and is not useful for HAMR. The efficiency varies slightly with the gap size when the outline dimensions and film thickness are fixed (optimized at $a = b = 500$ nm and $t = 100$ nm), as shown in Fig. 3(d). The percentage of the incident power dissipated in the central recording medium is about 0.55%, four fold smaller than the transmission efficiency due to the reflection from the media stack as well as transmission through the recording medium. Note that these efficiencies cannot be easily compared with values reported in the literatures,

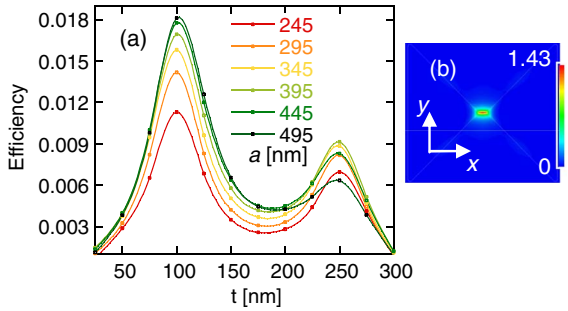


Fig. 4. (Color online) (a) Transmission efficiency as a function of dimensions $a$ and $t$, calculated on the exit side of the aperture with a region of 40 nm × 17 nm. (b) Heat absorption (MW/m$^3$) for a 495 nm bowtie aperture. $t = 100$ nm.

since the light source or the media stack used are all different, which all affect the calculation results.

### B. Generating Elongated Optical Spots Using Nanoscale Ridge Apertures

In magnetic recording, the recording bits are not in a circular shape [7], but have a bit aspect ratio of cross-track to down-track of about 3. Ridge apertures can be readily modified to generate elongated heat spots.

The bowtie aperture is investigated first. The gap shown in Fig. 1(b) is elongated and has dimensions of $s = 30$ nm and $d = 5$ nm. For this gap size, Fig. 4(a) shows the transmission efficiency as a function of the outline dimension $a$ and thickness $t$, with the highest efficiency of about 1.8% achieved at $a = 495$ nm and $t = 100$ nm and the corresponding heat spot is shown in Fig. 4(b). The FWHM spot size is 37.7 nm($x$) × 13.6 nm($y$) with an aspect ratio of 2.8.

A half-bowtie aperture [see Fig. 1(c)] is expected to produce similar results as a bowtie aperture. For example, it is found that the FWHM spot size varies little with the dimension $a$ when the gap dimensions ($s \times d$) are fixed. The hot spot also gets elongated when the ratio of $s$ to $d$ increases. For $s = 15$ nm and $d = 5$ nm, the FWHM spot size is about 37.1 nm($x$) × 16.2 nm($y$) and the aspect ratio is approximately 2.3 and for $s = 25$ nm and $d = 5$ nm, the FWHM is about 43.2 nm($x$) × 16.3 nm($y$), with an aspect ratio of 2.7. The heat spot for a 345 nm half-bowtie aperture is shown in Fig. 5(a) for $s = 15$ nm and $d = 5$ nm.

$C$ aperture [Fig. 1(d)] is a simple ridge aperture design, and can be considered as a half-bowtie aperture with straight ridge. It also exhibits a large field enhancement [19] and a high coupling efficiency when the recording medium is included [20,21].

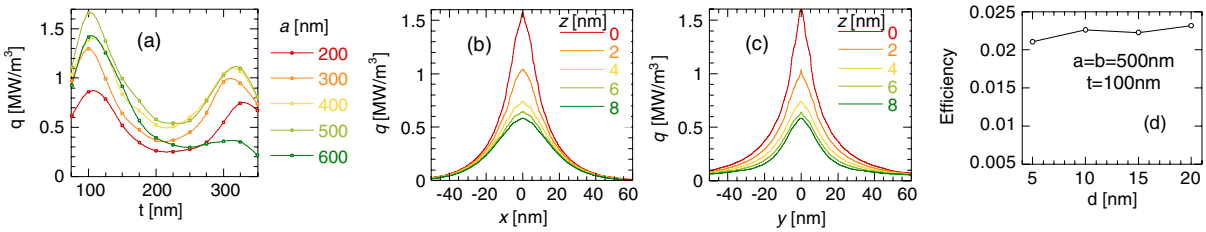


Fig. 3. (Color online) (a) Heat generation for different $t$ and aperture outline dimensions. Heat generation at different depths into the FePt layer in (b) $xz$ plane and (c) $yz$ plane. (d) Transmission efficiency as a function of the gap size.

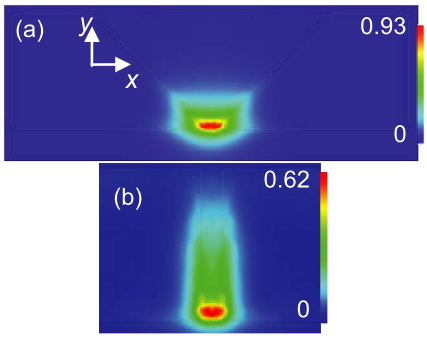


Fig. 5. (Color online) Heat spots (MW/m$^3$) for (a) a 345 nm long half-bowtie aperture, $t = 100$ nm, and (b) $C$ aperture, $a = 250$ nm, $b = 100$ nm, $t = 75$ nm. Both have $s = 15$ nm, $d = 5$ nm.

The result of the heat spot generated by the $C$ aperture is shown in Fig. 5(b), where $s = 15$ nm and $d = 5$ nm. However, it is seen that the heated region is elongated along the $y$ direction, due to the propagation of the surface plasmon along the Ag/air interfaces. Therefore, the $C$ aperture does not produce a heated spot with intended aspect ratio when the dimensions $s$ and $d$ are small.

### C. Improving Transmission of a Bowtie Aperture Using Circular Grooves

Extraordinary transmission has been demonstrated by placing periodic grooves around an aperture [22–25]. We investigate the transmission enhancement due to the addition of grooves using the bowtie aperture as an example. It is expected that similar results can be achieved using other apertures, including those for generating elongated spots. The incident Gaussian laser beam spot considered is 1 $\mu$m in radius, therefore, we consider the bowtie aperture with one groove only.

Figure 6 shows the schematic for a bowtie aperture with one groove in both top and cross-sectional views. The groove width in the metal film is larger than that in the substrate with $w_f = w_s + 100$ nm, considering the likely outcome of a metal deposition process. A 500 nm bowtie aperture is in the center with a square gap of 5 nm × 5 nm. The film thickness $t$ is 100 nm. The groove depth $v$ and the width of the groove $w_s$ are optimized to be 65 nm and 320 nm, respectively.

Figure 7(a) shows how the position of the groove $r_1$ and the width of the center post $w_0$ affect the

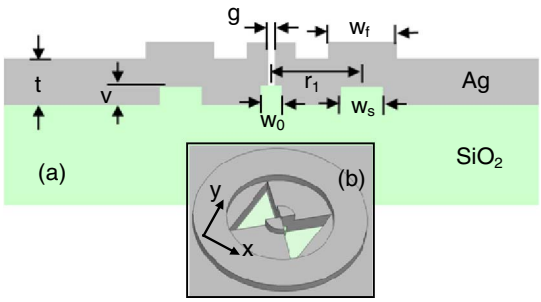


Fig. 6. (Color online) (a) Cross-section and (b) top views of bowtie aperture with one groove.

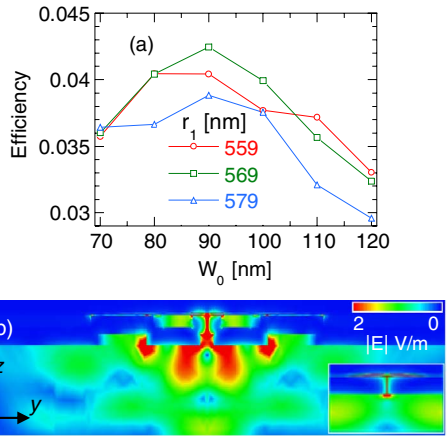


Fig. 7. (Color online) (a) Transmission enhancement for a 500 nm bowtie aperture with one groove as a function of $w_0$ and $r_1$. (b) Electric field on the $yz$ plane for the 500 nm bowtie aperture with one groove. The inset shows an identically sized bowtie without groove.

transmission efficiency. It can be seen that a higher field enhancement is achieved at $w_0 = 90$ nm and $r_1 = 569$ nm, with a transmission efficiency of about 4.3%. The enhancement factor is $4.3\%/2.1\% = 2$. The transmission enhancement is a result of surface plasmon polaritons and/or diffraction and their interactions with evanescent fields [26]. The electric field is shown in Fig. 7(b) and the inset is for a 500 nm bowtie aperture without groove. It is clear that the addition of one groove can collect more light to the center, which leads to a transmission enhancement. The resulting FWHM of the heat spot in the FePt layer is almost unaffected, about 19.3 nm($x$) × 19.8 nm($y$).

## 4. Conclusions

In summary, this work presents producing subdiffraction-limited optical spot using ridge apertures for heat-assisted magnetic recording. The computations are carried out with the presence of the recording medium. The half-bowtie and full bowtie aperture designs are found suited for generating an elongated heated spot to match the bit aspect ratio on the recording track. The transmission can be further enhanced by the addition of periodic grooves. We show that with one groove around the aperture, the near-field transmission can be doubled, with the transmission efficiency of about 4.3%.

The authors gratefully acknowledge the support of the Information Storage Industry Consortium (INSIC), the National Science Foundation (NSF) (grant no. DMI-0707817), the Defense Advanced Research Projects Agency (DARPA) (grant no. N66001-08-1-2037), and the United States Air Force Office of Scientific Research (USAFOSR)-Multidisciplinary University Research Initiative program (grant no. FA9550-08-1-0379).

## References

1. M. H. Kryder, E. C. Gage, T. W. McDaniel, W. A. Challener, R. E. Rottmayer, G. Ju, Y.-T. Hsia, and M. F. Erden, "Heat

Assisted Magnetic Recording," Proc. IEEE **96**, 1810–1835 (2008).
2. W. A. Challener, C. Mihalcea, C. Peng, and K. Pelhos, "Miniature planar solid immersion mirror with focused spot less than a quarter wavelength," Opt. Express **13**, 7189–7197 (2005).
3. C. Peng, C. Mihalcea, D. Buechel, W. A. Challener, and E. C. Gage, "Near field optical recording with a planar solid immersion mirror," Appl. Phys. Lett. **87**, 151105 (2005).
4. T. Rausch, C. Mihalcea, K. Pelhos, D. Karns, K. Mountfield, Y. A. Kubota, X. Wu, G. Ju, W. A. Challener, C. Peng, L. Li, Y.-T. Hsia, and E. C. Gage, "Near field heat assisted magnetic recording with a planar solid immersion lens," Jpn. J. Appl. Phys., Part 1 **45**, 1314–1320 (2006).
5. R. E. Rottmayer, S. Batra, D. Buechel, W. A. Challener, J. Hohlfeld, Y. Kubota, L. Li, B. Lu, C. Mihalcea, K. Mountfield, K. Pelhos, C. Peng, T. Rausch, M. A. Seigler, D. Weller, and X. Yang, "Heat-assisted magnetic recording," IEEE Trans. Magn. **42**, 2417–2421 (2006).
6. W. A. Challener, T. W. McDaniel, C. D. Mihalcea, K. R. Mountfield, K. Pelhos, and I. K. Sendur, "Light delivery techniques for heat-assisted magnetic recordings," Jpn. J. Appl. Phys. **42**, 981–988 (2003).
7. W. A. Challener, E. Gage, A. Itagi, and C. Peng, "Optical transducers for near-field recording," Jpn. J. Appl. Phys. **45**, 6632–6642 (2006).
8. W. A. Challener, C. Peng, A. V. Itagi, D. Karns, W. Peng, Y. Peng, X. Yang, X. Zhu, N. J. Gokemeijer, Y.-T. Hsia, G. Ju, R. E. Rottmayer, M. A. Seigler, and E. C. Gage, "Heat-assisted magnetic recording by a near-field transducer with efficient optical energy transfer," Nat. Photon. **3**, 220–224 (2009).
9. W. A. Challener, "Transducer for heat assisted magnetic recording," U.S. patent 7,272,079 (18 September, 2007).
10. L. Pan and D. B. Bogy, "Heat Assisted Magnetic Recording," Nat. Photon. **3**, 189–190 (2009).
11. HFSS 12.1, Ansoft LLC (2009).
12. E. D. Palik, *Handbook of optical constants of solid* (Academic, SanDiego, 1998).
13. E. X. Jin and X. Xu, "Finite-difference time-domain studies on optical transmission through planar nano-apertures in a metal film," Jpn. J. Appl. Phys. **43**, 407–417 (2004).
14. E. X. Jin and X. Xu, "Enhanced optical near field from a bowtie aperture," Appl. Phys. Lett. **88**, 153110 (2006).
15. L. Wang and X. Xu, "High transmission nanoscale bowtie-shaped aperture probe for near-field optical imaging," Appl. Phys. Lett. **90**, 261105 (2007).
16. L. Wang, S. M. Uppuluri, E. X. Jin, and X. Xu, "Nanolithography using high transmission nanoscale bowtie apertures," Nano Lett. **6**, 361–364 (2006).
17. Y. Kim, S. Kim, H. Jung, E. Lee, and J. W. Hahn, "Plasmonic nano lithography with a high scan speed contact probe," Opt. Express **17**, 19476–19485 (2009).
18. S. M. V. Uppuluri, E. C. Kinzel, Y. Li, and X. Xu, "Parallel optical nanolithography using nanoscale bowtie aperture array," Opt. Express **18**, 7369–7375 (2010).
19. X. Shi, L. Hesselink, and R. L. Thornton, "Ultrahigh light transmission through a *C*-shaped nanoaperture," Opt. Lett. **28**, 1320 (2003).
20. T. E. Schlesinger, T. Rausch, A. Itagi, J. Zhu, J. A. Bain, and D. D. Stancil, "An integrated read/write head for hybrid recording," Jpn. J. Appl. Phys. **41**, 1821–1824 (2002).
21. K. Sendur, C. Peng, and W. Challener, "Near-field radiation from a ridge waveguide transducer in the vicinity of a solid immersion lens," Phys. Rev. Lett. **94**, 043901 (2005).
22. H. J. Lezec, A. Degiron, E. Devaux, R. A. Linke, L. Martin-Moreno, F. J. Garcia-Vidal, and T. W. Ebbesen, "Beaming light from a subwavelength aperture," Science **297**, 820–822 (2002).
23. L. Martin-Moreno, F. J. Garcia-Vidal, H. J. Lezec, and T. W. Ebbesen, "Theory of highly directional emission from a single subwavelength aperture surrounded by surface corrugations," Phys. Rev. Lett. **90**, 167401 (2003).
24. E. C. Kinzel, P. Srisungsitthisunti, Y. Li, A. Raman, and X. Xu, "Extraordinary transmission from high-gain nanoaperture antennas," Appl. Phys. Lett. **96**, 211116 (2010).
25. D. Wang, T. Yang, and K. B. Crozier, "Optical antennas integrated with concentric ring gratings: electric field enhancement and directional radiation," Opt. Express **19**, 2148–2157 (2011).
26. H. J. Lezec, and T. Thio, "Diffracted evanescent wave model for enhanced and suppressed optical transmission through subwavelength hole arrays," Opt. Express **12**, 3629–3651 (2004).